Integrated summer insolation forcing and 40,000 year glacial cycles: the perspective from an icesheet/energy-balance model

Peter Huybers and Eli Tziperman

Dept. of Earth and Planetary Sciences, Harvard University, Cambridge MA

To be submitted to *Paleoceanography*.

Peter Huybers, Dept. of Earth and Planetary Sciences, Harvard University, Cambridge MA 02138 (phuybers@fas.harvard.edu)

Eli Tziperman, Dept. of Earth and Planetary Sciences and Division of Engineering and Applied Sciences, Harvard University, Cambridge MA 02138 (eli@eps.harvard.edu).

Although the origins of the 40,000 year glacial cycles during the early Pleistocene are readily attributed to changes in Earth's obliquity (also having a 40,000 year period), the lack of ice-volume variability at precession periods (20,000 years) is difficult to reconcile with most parameterizations of the insolation forcing. It was recently proposed that precession's influence on glaciation is muted because variations in the intensity of summer insolation are counterbalanced by changes in the duration of the summertime, but no climate model has yet been shown to generate obliquity period glacial cycles in response to the seasonal insolation forcing. Here we present a coupled icesheet/energy-balance-model that reproduces the seasonal cycle and, when run over long time periods, generates glacial variability in response to changes in Earth's orbital configuration. The model is forced by the full seasonal cycle in insolation, and its response can be understood within the context of the integrated summer insolation forcing.

The simple fact that obliquity's period is roughly twice as long as that of precession results in a larger amplitude glacial response to obliquity. But for the model to generate almost exclusively obliquity period glacial variability, two other conditions must be met. First, the icesheet's ablation zone must reside poleward of ∼60°N because insolation intensity is more sensitive to changes in Earth's obliquity at high latitudes. Second, the ablation season must be long enough for precession's opposing influences on summer and fall insolation intensity to counterbalance one another. These conditions are consistent with a warm climate and a thin icesheet, where the latter is simulated as a response to subglacial sediment deformation. If a colder climate is prescribed, or in the absence of basal motion, icesheets tend to be larger and undergo greater precession period variability, in keeping with proxy observations of late Pleistocene glaciation.

1. Introduction

That the ∼40,000 year glacial and temperature variability during the early Pleistocene [e.g. *Shackleton and Opdyke*, 1976; *Pisias and Moore*, 1981; *Shackleton and Hall*, 1984; *Raymo et al.*, 1989; *Ruddiman et al.*, 1989; *Imbrie et al.*, 1993; *Tiedemann et al.*, 1994; *Venz et al.*, 1999; *Liu and Herbert*, 2004; *Huybers*, 2007; *Lawrence et al.*, 2006] are in some way related to the 40,000 year changes in Earth's obliquity seems almost certain, but such a description is incomplete. The caloric summer half year [e.g. *Milankovitch*, 1941] and the insolation intensity on any summer day [e.g. *Hays et al.*, 1976; *Imbrie et al.*, 1992] varies primarily with the precession of the equinoxes, or at ∼20,000 year periods (assuming that the eccentricity of the Earth's orbit is not anomalously small). Why, then, is there not more precession period variability during the early Pleistocene?

Kukla [1968] as well as *Muller and MacDonald* [2000] speculate that the driver of glaciation may be winter insolation at 65°N, sensitive primarily to obliquity because it dictates whether 65°N experiences polar night. But while this yields an insolation quantity having the correct time-scale, it is difficult to rationalize how winter insolation variability could affect glaciation, both because no ablation is expected in the winter and the amplitude of the variability is much smaller than for summer. Another quantity sensitive primarily to obliquity is the meridional insolation gradient [*Berger*, 1978; *Young and Bradley*, 1984; *Johnson*, 1991; *Raymo and Nisancioglu*, 2003]. Increasing obliquity causes an annual average redistribution of insolation from latitudes equatorward of 44°N to latitudes poleward of this hinge point, whereas precession causes insolation to change more uniformly with latitude. *Raymo and Nisancioglu* [2003] proposed that insolation gradients would modulate the poleward transport of moisture and heat and thereby determine glacial mass balance, but model simulations suggest that the obliquity-induced variations in the insolation gradient have a minor influence on glaciation [*Jackson and Broccoli*, 2003; *Nisancioglu*, 2004]. Another suggestion [*Ashkenazy and Tziperman*, 2004] is that early Pleistocene glacial cycles are nonlinear oscillations with an intrinsic period close to 40 Ky, and that these become phase-locked to the obliquity-forcing[*Gildor and Tziperman*, 2000; *Tziperman et al.*, 2006].

A more recent hypothesis calls upon how glacial variability is recorded to mute the precession signal. *Raymo et al.* [2006] suggest that precession period variations in glaciation are anti-symmetric between the hemispheres, but whose effects are averaged in the oceans and thus absent from records of marine calcite δ^{18}O. To explain why precession variability is not present in ice-rafted debris records from the North Atlantic [e.g. *Shackleton and Hall*, 1984; *Ruddiman et al.*, 1989] and Nordic Seas [e.g. *Jansen et al.*, 2000], which covary with δ^{18}O at predominantly 40Ky periods, *Raymo et al.* [2006] call upon delivery of ice-rafted debris to occur only during obliquity induced excursions in sea-level and not during precession induced ablation events. Note, however, that North Atlantic sea-surface [*Ruddiman et al.*, 1989], intermediate [*McIntyre et al.*, 1999], and deep water temperatures [*Dwyer et al.*, 1995] all appear to vary at 40Ky periods. Also, ice-volume appears to have varied at 40,000 year periods prior to the glaciation of Antarctica [*Zachos et al.*, 2001], indicating that at some point in Earth's history a mechanism existed for causing Northern Hemisphere icesheets to vary primarily at obliquity periods.

Lastly, it has been suggested by one of the authors [*Huybers*, 2006] that the absence of precession period variability during the early Pleistocene occurs because the Earth's distance from the sun is inversely proportional to its angular velocity, i.e. Kepler's second law. Annual ablation is expected to be a function of both the solar radiation intensity (related to Earth's distance from the sun) and the duration of the ablation season (related to Earth's angular velocity). These two influences are both taken into account by integrating insolation intensity over the time variable duration of the summer, a quantity referred to as the summer-energy. In this case, summer is defined as the period during which daily average insolation intensity exceeds a specified threshold. The summer-energy is generally insensitive to precession because, for example, just when perihelion occurs at summer solstice, summertime is shortest. That is, Kepler's second law dictates that duration and intensity counter-balance one another. Here we elaborate on what controls the glacial sensitivity to changes in obliquity and precession using a coupled icesheet/energy-balance-model.

Numerous studies have used numerical models to explore glacial variability, but for such a model to address the summer-energy hypothesis requires the representation of both the full seasonal cycle and the secular variations in precession, obliquity, and eccentricity — thus spanning five orders of magnitude in time-scales. We are aware of only four previous studies which include the full seasonal cycles and attempt to simulate 40Ky glacial cycles. *Berger and Loutre* [1997] developed a model having zonally averaged ocean and land components coupled to a parabolic icesheet. It generated glacial variability of roughly equal magnitude at obliquity and precession periods during the early Pleistocene as well as considerable energy spread across a continuum of timescales. *Nisancioglu* [2004] coupled a zonally averaged atmospheric energy balance model, including a representation of moisture and heat transport, to a parabolic icesheet model and obtained somewhat greater precession than obliquity period variability. *Jackson and Broccoli* [2003] coupled an atmospheric GCM to a slab ocean and ran it to equilibrium under various orbital configurations. As their model did not include an icesheet, they analyzed variations in precipitation and positive degree days and, again, find somewhat more precession than obliquity period variability. Finally, *DeConto and Pollard* [2003a, b] employed a coupled atmospheric GCM and icesheet model to represent Antarctica. While their focus was on initiation of glaciation in Antarctica, the orbital period fluctuations in ice-volume appear (from visual inspection of their figures) to be almost exclusively at obliquity periods. It should be noted, however, that to speed-up the model integration, idealized variations in orbital parameters were used wherein obliquity and eccentricity variations were approximated to have periods which are integer multiples of the precession cycle, making it difficult to interpret sensitivities to the individual orbital parameters.

Raymo et al. [2006] point out that no climate model has simulated the 40,000 year glacial cycles as a response to the full insolation forcing: a fair challenge to any hypothesis seeking to explain the record of early Pleistocene glacial variability as directly indicating variations in ice-volume. Here we present a coupled icesheet/energy-balance-model which calculates ablation as a function of the surface energy balance and is driven by the full seasonal cycles of insolation — sensitive to both precession and obliquity. The model generates 40 Ky glacial cycles consistent with the early Pleistocene observations and the predictions of the summer energy. We first describe some features of the summer energy and then discuss results from the model.

2. Summer-energy

The concept of positive degree days (PDDs) provides a simple relationship between temperature and glacial ablation [*Braithwaite and Zhang*, 2000],

$$\mathrm{PDD} = \sum \delta_d T_d. \tag{1}$$

Here T_d is the daily temperature and δ_d is zero if $T_d < 0°\mathrm{C}$ and one otherwise. The summer-energy is defined in close analogy with PDDs, as the sum of the insolation intensity exceeding a threshold,

$$J = \sum_{d=1}^{365} \beta_d \Phi_d, \tag{2}$$

where Φ_d is the daily average insolation intensity, and β_d is one when Φ_d is above a threshold, τ; otherwise, β_d is zero. Note that the full magnitude of the insolation intensity — not only the portion above the threshold — is summed under the assumption that most incident radiative energy will eventually lead to ablation once the freezing point is obtained. In order to provide a conceptual framework by which to interpret the model results, which are presented in subsequent sections, it is useful to first explore how summer-energy depends on latitude and the threshold. *Huybers* [2006] only discussed summer-energy at 65°N with a threshold of 275 W/m^2.

The variance of the summer-energy, computed between 2-1Ma, ranges from zero to (3000 Giga-Joules/m^2)^2, depending on the threshold and latitude (Figure 1a). Variance in J is greatest when the threshold is just below the maximum insolation received at each latitude, partly because insolation intensity is large but also because the time rate of change in insolation is small — shifts in insolation intensity then cause relatively large changes in the number of days exceeding the threshold. In the tropics and mid-latitudes there is negligible summer-energy variability at low thresholds because intensity exceeds τ all year, and only changes in the annual average intensity influence J. Nearly all the summer-energy variance is partitioned between the obliquity and precession bands (Figure 1b,c). Obliquity dominates at most threshold values below about 200 W/m^2 because insolation is integrated over nearly the whole of the year and precession has no influence on annually integrated insolation [*Rubincam*, 1994]. An exception is at 44°N and nearby latitudes, where shifts in Earth's obliquity have negligible influence on annual insolation, leaving only the small contribution from changes in eccentricity. At latitudes above 60°N, presumably the most relevant for determining the extent of glaciation, J is primarily a function of obliquity up to thresholds of 350 W/m^2.

The switch from obliquity to precession period variability at thresholds above 350 W/m^2 can be understood by considering the change in the structure of the annual cycle resulting from the precession of the equinoxes. When perihelion (i.e. Earth's closest approach to the sun) occurs in Northern Hemisphere summer, the insolation intensity increases between May and August but decreases between September to November (Fig. 2). This fall deficit owes to the fact that summer perihelion is associated with Earth being unusually far along its orbital path. Low threshold values tend to intersect the insolation intensity curve in the fall, and therefore summer perihelion causes a reduction in the number of days during which insolation intensity exceeds τ. Thus, the increased intensity associated with summer perihelion is counterbalanced by a decrease in exposure time, giving a summer-energy nearly independent of precession. Higher threshold values, however, intersect the insolation intensity curve between July and August, in which case summer perihelion causes an increase in insolation intensity as well as duration and a corresponding increase in summer-energy. Note that, following convention, the year is defined with respect to Northern Hemisphere Spring Equinox.

There exists a conspicuous valley bisecting the precession period variability in Figure 1c. The lobe of precession variability associated with higher thresholds is intensity controlled, i.e. maxima in summer energy are associated with perihelion occuring during summer. Conversely, the lobe of precession variability at low thresholds is durationally controlled, i.e. summer-energy is largest when aphelion (Earth's furthest excursion from the sun) occurs during summer. The intervening valley is where summer-energy maxima occur for both summer aphelion and summer perihelion, giving a period of half a precession cycle, or $\sim$11Ky.

The latitude-threshold space in which an icesheet's ablation zone exists helps determine the ratio of obliquity to precession period variability. When ablation occurs at thresholds below $\sim$350 W/m^2 and at latitudes above 60°N, glaciers are expected to be most sensitive to changes in Earth's obliquity. Moving the ablation zone equatorward or requiring a higher ablation threshold would increase the precession period variability. These inference are further explored in the following sections using a coupled icesheet/energy-balance-model.

3. Model description

The model formulation is similar to that presented by *Pollard* [1978], asynchronously coupling an energy-balance-model (EBM) and an icesheet (see Fig. 9). The EBM is zonally averaged and spans the equator to the pole at one degree resolution. Atmospheric heat transport is parameterized using the formulation of *Stone* [1972]. Ablation is computed as a function of surface energy balance, as opposed to the positive degree day formulation, which would largely presuppose the validity of the summer-energy concept. The hydrological cycle is treated very simply, ignoring latent heat fluxes, and assuming that a constant amount of ice accumulates each day for which the atmospheric surface temperature is below freezing; otherwise precipitation falls as rain and is assumed to run-off. The EBM state appears to be an unique function of orbital configuration and icesheet topography and converges to a stable seasonal cycle within a few years. The annual ice mass-balance is computed at each grid box from the equilibrated EBM and then used to force an icesheet.

The icesheet model is also zonally averaged and the domain spans 30°N to 85°N, outside of which calving is assumed to impose zero ice-thickness boundary conditions. Ice deformation is calculated from horizontal stress according to Glen's flow law. Early Pleistocene icesheets may have been as spatially expansive as during the late Pleistocene [*Boellstorff*, 1978; *Fisher et al.*, 1985; *Joyce et al.*, 1993] (but see *Barendregt and Irving* [1998]), while ice-volume variations appear to have been smaller (e.g. *Pillan, Chappell and Naish* [1998] and as indicated by δ^{18}O, Fig. 2c,e). A possible resolution is that a deformable bed underlaid the Laurentide during the early Pleistocene and led to faster flowing, more expansive, and thinner icesheets [*Fisher et al.*, 1985; *Beget*, 1986; *Alley*, 1991; *Clark and Pollard*, 1998]. In this study we assume the icesheet rests atop a layer of deformable sediment, represented using the model of *Jenson et al.* [1996]. The presence of deformable sediment is, however, not necessarily required as a thin icesheet could also result from basal sliding in response to the presence of melt water [*Jenson et al.*, 1996].

A detailed description of the model is provided along with a list of the specified parameters (see Appendix A). Parameter values are selected to give reasonable agreement with the modern climate system (see Appendix B). At certain points it will be useful to demonstrate model behavior under different parameterizations, involving changes in surface temperature and the deformability of sediment; all these deviations from the "standard" parameterizations are explicitly stated.

3.1. 40Ky glacial variability

While the model is seasonally ice-free under modern orbital conditions, orbitally induced shifts in the insolation at the top of the atmosphere are sufficient to initiate glaciation. 82% of the variance in ice-volume is within the obliquity band ($1/41 \pm 1/150$ Ky^{-1}) and only 12% at the precession band ($1/21.1 \pm 1/150$ Ky^{-1}) (see Figure 3). The remainder of the ice-volume variance is spread throughout a continuum of timescales. The partition of variance in the composite δ^{18}O records of [*Huybers*, 2007] for the same time period is 54% of the variance in the obliquity band and 2% in the precession band. A similar partition is found in the composite δ^{18}O record of [e.g *Lisiecki and Raymo*, 2007]. The lower fractions of variance in the δ^{18}O orbital bands relative to the model orbital bands is anticipated from some combination of age-model error [e.g. *Huybers and Wunsch*, 2004], observational noise, the fact that Earth's climate variability comprises myriad stochastic phenomena not included in the model, that δ^{18}O is also sensitive to changes in temperature, and that approximately 80 Ky long glacial cycles are found near 1.6 and 1.2 Ma in the δ^{18}O record — associated with a concentration of variability near 1/80 Ky. The bottom line is that the model results are consistent with the observation of negligible precession period variability during the early Pleistocene (Figure 3c). There are more nuanced discrepancies between the δ^{18}O record and the model results, and these are addressed in more detail in Secs. 4 and 5.

The size of the model icesheet is in rough agreement with estimates for 50m amplitude sealevel variations during the early Pleistocene [e.g. *Pillan, Chappell and Naish*, 1998]. At its maximum extent the model icesheet spans 60° to 85°N with an average thickness of 1500m (Figure 4). Although longitude is not represented, if we assume the icesheet spanned N. America, ∼3000km at high latitudes, the icesheet's volume corresponds to ∼40m of sealevel. During maximum glacial extent the annual average temperatures at high latitudes decrease by approximately 20°C from an interglacial to glacial state, primarily owing to changes in albedo and surface height. Decreased temperatures leads to greater accumulation as more of the precipitation falls as snow, and which is balanced by increased ablation at more equatorward and warmer latitudes. Ablation occurs almost exclusively at the leading edge of the icesheet as this region receives relatively more insolation, is associated with the largest flux of heat from the atmosphere, and is at a low elevation.

Glaciation is controlled in the model by orbital variations in two senses. First, model runs starting from different initial conditions all converge within a few glacial cycles. Second, in the absence of orbital or stochastic variations the model would reach a steady-state with either a permanent icesheet or seasonally ice-free conditions. In the presence of substantial noise and orbital variations, the model produces fluctuations in ice-volume similar to when it is forced only by orbital variations. For example, when a noise term is introduced into the ice mass balance having a standard deviation of two meters (twice the maximum precipitation signal), the model continues to undergo 40Ky glacial cycles. In this case, the noise is uncorrelated at the 1° grid-spacing and five year time-step of the ice-sheet model. The icesheet apparently acts as a very effective smoother in space (redistributing ice-mass anomalies) and time (being largely insensitive to high-frequency anomalies) so that the low-frequency systematic changes induced by insolation still dominate the result. This damping of high-frequency variability may explain why the early Pleistocene glacial cycles appear to occur so regularly at 40Ky intervals, even in the presence of the inevitable stochastic variability.

This description of the model behavior still leaves the question of why the model generates primarily 40 Ky glacial variability? As a partial answer, consider the insolation threshold at which ablation is induced in the model. Fig. 5 shows an estimate of this threshold, obtained by sampling the minimum insolation at which ablation occurs as a function of latitude and elevation. Ablation always occurs at latitudes above 60°N and initiates at insolation intensities below 320 W/m^2. These are just the conditions under which summer-energy was shown to vary primarily at the obliquity period (see Sec. 2).

Thus, in so much as summer energy and the model behave similarly, obliquity period variability is expected.

3.2. Sensitivity experiments

Three sensitivity studies are used to illustrate the differences between how the model responds to obliquity and precession.

Thin static icesheet: In the first sensitivity experiment a ten meter thick ice-field is specified to extend from 60°N to 85°N. Increasing obliquity from a minimum (22.1°) to maximum (24.5°) results in an increase in insolation of 25 W/m^2 at high latitudes during the summer and a decrease in mass balance of −0.43 m/y, when spatially averaged over the ice-field (Fig. 6a,b). The change in mass-balance comes from increased ablation (−0.41 m/yr) and a small decrease in accumulation (−0.02 m/yr). (Changes in accumulation would probably play a more prominent role if precipitation rates were made to depend on the climate [e.g. *Gildor and Tziperman*, 2000].) When perihelion is shifted from winter to summer solstice and the long-term eccentricity average of 0.0275 is specified, insolation intensity increases in the spring and early summer by as much as 80 W/m^2 but decreases by a corresponding amount in the later summer and fall (as also described in Section 2). Likewise, mass balance decreases in the early part of the ablation season but increases in the later part of the ablation season, leading to a low sensitivity of −0.18 m/yr, or less than half that associated with obliquity (Fig. 6d,e).

Thick static icesheet: In the second sensitivity study, the icesheet elevation is increased to 1500 meters, resulting in a temperature decrease of 10°C at the icesheet surface.

The sensitivity to obliquity decreases by a factor of two to -0.22 m/yr, but the sensitivity to precession only decreases by roughly 20%, to -0.14 m/yr (Fig. 6c,f). The sensitivity to precession is less influenced by the colder temperatures because no ablation occurs during the fall and the counterbalancing effect is lost. The change in sensitivity between the thin and thick icesheet runs parallels the changes anticipated in the summer energy between specifying a low and high threshold value.

Dynamic icesheet: An alternative method to compute sensitivity is to average the mass-balance associated with minima in obliquity and subtract this from the average maximum-obliquity mass-balance. Averages are taken from a model run spanning 2 to 1 Ma. The mass-balance sensitivity to obliquity, averaged between 65°N and 85°N, is -0.41 m/yr, and for precession the sensitivity is -0.16 m/yr. The ratio between obliquity and precession variance is obtained by squaring the ratio of the sensitivities$(-0.41/-0.16)^2 =$ 6.6, in good agreement with the spectral distribution of energy obtained from the model run (0.82/0.12=6.8, Fig. 3b).

The sensitivity to obliquity is larger in the dynamic than the static icesheet runs. This suggests that the time-dependence of the model also plays a role in determining the ratio of obliquity to precession related variance, a topic taken up in more detail in the next section.

3.3. Consequences of a non-equilibrium response to astronomical forcing

A coherence analysis shows that model ice-volume variations are almost perfectly coherent with the changes in obliquity as well as precession, lagging these orbital variations by approximately 90°. This is consistent with observational studies of the marine δ^{18}O record as well as dynamical expectations [*Imbrie and Imbrie*, 1980; *Huybers*, 2006; *Roe*, in press], and suggests that insolation does not control the magnitude of ice-volume, but instead its rate of change. A simplification of this relationship is,

$$\frac{dV}{dt} = A_{\text{obl}} \cos(w_{\text{obl}} t) + A_{\text{prec}} \cos(w_{\text{prec}} t). \tag{3}$$

The two terms on the right hand side represent the influence of obliquity and precession, having frequencies of $w_{\text{obl}} = 1/41$ Ky^{-1} and $w_{\text{prec}} = 1/22$ Ky^{-1} respectively. The difference in phasing as well as the frequency and amplitude modulations of the orbital forcings have been ignored; their inclusion would not alter the point being made here. Integrating gives,

$$V = \frac{A_{\text{obl}}}{w_{\text{obl}}} \sin(w_{\text{obl}} t) + \frac{A_{\text{prec}}}{w_{\text{prec}}} \sin(w_{\text{prec}} t), \tag{4}$$

so that ice-volume lags behind the cosine forcing terms by 90°, consistent with observations. The amplitude of the ice-volume variability depends on the frequency of the forcing, and ice-volume is almost twice as sensitive to obliquity as to precession, $w_{\text{prec}}/w_{\text{obl}}$=1.9.

Is this simple representation of reasonable? The spatial and temporal structure of the obliquity and precession insolation anomalies are distinct. Obliquity induced changes in insolation contain low-frequency components (e.g. $1/41$ Ky^{-1}), whereas precession variations only alter the structure of the seasonal cycle [*Rubincam*, 1994]. To more fully explore the influence of different periods of forcing upon amplitude of the ice-volume response, a series of model runs are performed using idealized, sinusoidal variations in orbital parameters ranging in period from 10Ky to 100Ky (Fig. 7). As anticipated from

Eq. 4, the amplitude of ice-volume variations is found to generally be proportional to the period, although the relationship breaks-down at periods longer than 50Ky. The break-down seems to arise because of the physical limits in the icesheet extent. For example, under constant low obliquity (corresponding to an infinite period) the icesheet eventually grows to a steady state limit reaching to 50°N. In a somewhat cooler climate ice-sheet volume would be larger, on average, but the scaling with respect to forcing frequency behaves similarly. Thus, both observations and the model indicates that the amplitude of the orbital response depends on the forcing period.

The predominance of the obliquity period variability can apparently be explained as a result of both counter-balancing of the precession effect and a larger obliquity response because of its lower frequency. It is possible to quantify the relative importance of these mechanisms. The obliquity-induced changes in insolation intensity at high-latitudes are roughly a third those caused by precession. However, for the case of a static icesheet, model mass-balance was found to be more sensitive to obliquity, suggesting that the influence of precession is reduced by about a factor of four by seasonal counter-balancing. Obliquity also has a period roughly twice as long as precession suggesting another factor of two. Multiplying the relative influences and squaring gives a ratio between the expected variance of obliquity and precession, $(1/3 \times 4 \times 2)^2 \approx 7$, consistent with the 7:1 partition of variance between obliquity and precession found in the model run.

4. The effect of a cooling climate and implications for the late Pleistocene

The climatic response to orbital variations itself depends on the background state of the climate. Cooling the climate is expected to be analogous to increasing the threshold for ablation in the summer energy parameterization and thus increase the relative fraction of precession period variability. To check this inference, a cooler surface temperature is induced in the model by decreasing the emission level for outgoing longwave radiation. This decreases the effective thickness of the atmosphere with respect to longwave radiation and is similar to decreasing greenhouse gas concentrations [see e.g. *Goody*, 1995]. The average surface temperature in the model decreases by $\sim 1°C$ for each 100m the emission level is lowered, both because of increased transmission of longwave radiation to space and because of feedbacks involving an increase in the area and thickness of the icesheet. Precession variability increases monotonically with cooling surface conditions. For example, when the emission level is lowered from 7km to 6.5Km, the mean temperature over the icesheet cools by 5°C (partially suppressing ablation during the late summer and fall), and 50% of the ice volume variance is concentrated at the precession periods (see Fig. 8).

The increase of precession period glacial variability with a cooling climate owes to three interrelated effects. First, the direct cooling of the ablation zone restricts ablation to a shorter portion of the summer so that the counterbalancing between summer and fall insolation changes is lost (see Secs. 2 and 3.2). Second, the cooler climate leads to a thicker icesheet, which is associated with further cooling of the surface. Finally, the cooler climate also permits icesheets to reach further equatorward, and while this would normally be associated with a warmer climate, the insolation at lower latitudes is more sensitive to variations in precession. Conversely, raising the emission level to 7.1km further suppresses precession period variability, though if the surface temperatures are made still warmer, glaciation is suppressed all together.

Another model run is presented to illustrate how changes in basal conditions can also evoke precession period variability. The deformable till at the base of the glacier is set to zero thickness so that no basal motion occurs. The average slope associated with the leading edge of the icesheet increases from 0.0003 m/m to 0.02 m/m (significant ablation at the margin sustains this very steep slope). Although the model lacks sufficient resolution to accurately model the ablation zone, such an effect is in the correct direction, with the much steeper ascent leading to a smaller ablation zone, and permitting the icesheet to move equatorward to 50°N. The icesheet is now almost exclusively sensitive to changes in precession, which accounts for 85% of the ice-volume variance. The loss of ablation zone area also makes the icesheet less sensitive to insolation variations — changes in precession cause only 0.1% changes in net ice-volume. Thus, in the absence of basal motion, the model icesheet is largely insensitive to orbitally induced shifts in insolation. This is consistent with coupled icesheet/energy-balance-models generally yielding meager variations in ice-volume in direct response to insolation shifts [e.g. *Oerlemans*, 1984], except when unrealistically large ice-deformability is specified [e.g. *Weertman*, 1976; *Pollard*, 1978]. Furthermore, the apparent need for a thin icesheet in order to obtain predominantly obliquity period variability may explain why earlier modeling studies [*Berger and Loutre*, 1997; *Nisancioglu*, 2004] which simulated the full seasonal cycle and a dynamic icesheet, but not basal sliding, obtained substantial precession period variability.

The model generates greater ice-volume and more precession period variability in response to climate cooling. Thus the progression of glacial variability over the last few million years toward greater ice-volume and greater precession period variability [e.g. *Huybers*, 2007] can be understood as the glacial response to to a cooling climate [e.g. *Shackleton and Hall*, 1984; *Raymo*, 1994; *Ravelo et al.*, 2004]. The model also generates larger icesheets and a greater fraction of precession period variability when the icesheet's basal motion is stopped [e.g. *Clark and Pollard*, 1998]. The model does not permit differentiating between the two scenarios, although they may be related as a cooler climate would tend to suppress basal melting. The model fails, however, to generate some of the key features of late Pleistocene glacial cycles, for example, not sufficiently deglaciating and not generating ∼100Ky variability.

There are also some shortcomings in the model's simulation of early Pleistocene glacial variability. Using δ^{18}O records as a proxy for ice-volume, *Hagelberg et al.* [1991] and *Lisiecki and Raymo* [2007] have shown that the climate increasingly resides in a glacial state towards the present, and *Ashkenazy and Tziperman* [2004] and *Huybers* [2007] showed that the asymmetry between rapid deglaciation and slow reglaciation is present during the early Pleistocene and increases toward the present. The model glacial cycles, however, are symmetric, appearing most similar to the glacial cycles near ∼2 Ma.

Another shortcoming is that the maximum equatorward extent of the model icesheet is only 60°N whereas icesheets seem to have reached into Iowa and Nebraska (40°N, *Boellstorff* [1978]; *Barendregt and Irving* [1998]) and there are indications that the Laurentide repeatedly entered the Mississippi River drainage basin during the early Pleistocene [*Joyce* *et al.*, 1993]. Perhaps the glacial cycles generated by this model represent a simple prototype, but other mechanisms associated with trends toward increasing asymmetry, larger amplitude and longer period glacial cycles and episodes of more southerly glacial extent must also be present. Indeed, a more complex and episodic relationship with insolation forcing seems necessary if one is to explain the obliquity cycle skipping and ~100Ky glacial cycles of the late Pleistocene.

5. Summary and conclusions

Insolation integrated over the time-variable summer period, termed the summer energy, provides a framework by which to understand the partition of glacial variability between obliquity and precession periods. This partition is a function of the latitude and ablation threshold. A higher threshold indicates that greater insolation intensity is required to cause ablation. Summer-energy predicts that an icesheet will be most sensitive to obliquity when its ablation zones exists at high latitudes and undergoes ablation at low insolation thresholds. Obliquity control occurs because it has a larger influence on insolation at higher latitudes and the low thresholds permit counterbalancing between the opposing precession-induced insolation anomalies in summer and fall [*Huybers*, 2006].

An icesheet/energy-balance-model is constructed to explore the relationship between insolation and ice-volume in more detail. The model approximates the modern seasonal cycle in temperature, albedo, and energy fluxes, and when integrated over long time periods, variations in Earth's orbital configuration lead to 40 Ky glacial cycles extending southward as far as 60°N. Ablation is calculated according to a surface energy balance and is shown to initiate at an insolation threshold depending on latitude and elevation. The insolation threshold always resides within the parameter range in which summer-energy predicts primarily obliquity period variability. Furthermore, sensitivity to precession is muted because ablation anomalies are counterbalanced between summer and fall, as anticipated from the summer-energy.

Another reason why model glaciation is controlled by obliquity owes to its longer period relative to precession. The insolation forcing determines the rate of change of ice-volume, not its magnitude, suggesting that the amplitude of the response will be proportional to the forcing period, and as demonstrated by model simulations. Thus ice-volume is about twice as sensitive to a 40Ky obliquity periods as compared to a 20Ky precession period.

The focus is on the origins of the early Pleistocene 40 Ky glacial cycles, but we hope that study of these seemingly simpler variations will also facilitate understanding of the late Pleistocene glacial cycles. When the longwave emission level of the atmosphere is lowered, temperature decreases, the icesheet becomes thicker, and it extends further south — all of which tends to increase precession period variability. Likewise, in the absence of basal deformation, the icesheet becomes thicker, extends further south, and is relatively more sensitive to changes in precession. Greater precession period variability and larger icesheets during the late Pleistocene can thus readily be explained as the response to either a cooler climate or less basal deformation.

The model runs conducted with a cooler climate or with basal sliding switched-off also indicate a deficiency in the present model, whereby larger icesheets grow but never completely deglaciate. Furthermore, the 40 Ky variations produced by the model are symmetric, indicating a mostly linear response to Milankovitch forcing, consistent with the early 40 Ky glacial cycles, but not with the asymmetry of the later glacial cycles [*Ashkenazy and Tziperman*, 2004]. The model also fails to produce trends toward greater amplitude or to skip one or two obliquity forcing cycles prior to deglaciation [*Huybers and Wunsch*, 2005; *Huybers*, 2006], all of which indicates that at least one mechanism is missing.

A number of mechanisms have been suggested to account for the deglaciation of large icesheets, and which could also introduce asymmetries as well as skipping of obliquity cycles. *Oerlemans* [1980] showed that if a long time-constant is prescribed for isostatic adjustment (10 Ky), rapid deglaciations can be made to occur once an icesheet has sufficiently depressed its underlying bed, and that this can generate self-sustained $\sim$100 Ky glacial cycles. *Pollard* [1982] speculated that sea-water incursion at the base of an icesheet or that calving associated with proglacial lakes would increase deglaciation. Using a thermo-mechanical icesheet model, *Oerlemans* [1984] suggested that episodic production of basal melt water could lead to rapid collapse of an icesheet. *Peltier and Marshall* [1995] called upon dirty snow to lower ice-albedo. *Gildor and Tziperman* [2000] argue sea-ice growth during a glaciated state would diminish accumulation and eventually starve an icesheet. There is no shortage of mechanisms for generating complete deglaciations, and much of the future work lies in distinguishing between these plausible hypotheses.

Acknowledgments

We thank Nick Pisias and Lorraine Lisiecki for constructive reviews. This work was supported by the McDonnell Foundation and by the NSF paleoclimate program, grant ATM-0455470.

Appendix A: Details of the model

Our aim is to construct a model capable of representing insolation's influence on glaciation. Presently, owing to computational constraints, atmospheric GCMs can usually only take of a series of snapshots of the climate state through a glacial cycle [e.g. *Jackson and Broccoli*, 2003] or must utilize idealized variations in Earth's orbit [e.g. *DeConto and Pollard*, 2003a]. Thus, following a long tradition [e.g. *Pollard*, 1978; *North et al.*, 1981; *Shell and Somerville*, 2005], we couple an energy balance model (EBM) and an ice-sheet model (see Fig. 9).

A1. Energy balance model

The EBM explicitly represents temperature at three-levels: the middle atmosphere (T_a), surface (T_s), and subsurface (T_{ss}). Temperature at each level responds to fluxes of energy,

$$C_a \frac{\partial T_a}{\partial t} = S_a + I_a + F_s + D_a, \tag{A1}$$

$$C_s \frac{\partial T_s}{\partial t} = S_s + I_s - F_s + F_{ss}, \tag{A2}$$

$$C_{ss} \frac{\partial T_{ss}}{\partial t} = -F_{ss}, \tag{A3}$$

where C is the heat capacity associated with each layer, t is time, S is the solar (shortwave) heating, and I is the infrared (longwave) heating. F_s is the sensible heat flux from the surface to the atmosphere, and F_{ss} is the heat flux from the subsurface into the surface.

Latent heat fluxes and transport of heat within the ground and ice are not represented. There is no ocean, except as implied by the icesheet calving off at continental margins and the prescription of an ice-albedo in keeping with sea-ice at the highest latitudes. Values for each constant are given in Table 1.

The incoming solar radiation is variously absorbed and reflected by the atmosphere and surface, depending on the reflectivity (R), absorptivity (A), and transmissivity (T) of the atmosphere and albedo (α) of the surface. Separate albedos are specified for ice (α_i) and bare ground (α_g). The solar energy absorbed by the atmosphere is,

$$S_a = AS + \frac{TS\alpha_{(i,g)}A}{1-\alpha_{(i,g)}R}, \tag{A4}$$

where the denominator accounts for absorption of radiation reflected by the surface multiple times. The solar radiation absorbed by the surface is,

$$S_s = TS\frac{1-\alpha_{(i,g)}}{1-\alpha_{(i,g)}R}. \tag{A5}$$

A, R, and T are influenced by clouds and water-vapor and are expected to change with a changing climate but here, for simplicity, are parameterized as fixed constants. The sum, $A+R+T$, must equal one. Incoming solar radiation, S, is calculated using the approach of *Berger* [1978] and the orbital solution of *Berger and Loutre* [1992].

The vertical profile of temperature in the atmosphere is approximated as having a constant moist adiabatic lapse rate, Γ_m. The alternative of specifying a spatially and, possibly, temporally varying lapse rate would require further assumptions regarding the hydrological cycle which we choose to circumvent. The lapse rate is used to calculate the temperature at the atmospheric surface layer, $T_{as} = T_a + \Gamma_m H_{as}$, where H_{as} is the distance from the middle atmosphere to the surface and which varies according to icesheet thickness and surface depression.

The surface exchanges longwave radiation with the atmosphere according to their respective temperatures,

$$I_s = \epsilon_a \sigma T_{as}^4 - \sigma T_s^4. \tag{A6}$$

Here ϵ_a is the atmospheric emissivity, the surface emissivity is assumed to be one, and σ is the Stefan-Boltzmann constant. Atmospheric longwave radiation fluxes are given by,

$$I_a = \epsilon_a \sigma T_s^4 - \epsilon_a \sigma T_{as}^4 - \epsilon_a \sigma T_{ul}^4. \tag{A7}$$

The final term on the right is the emission temperature of the upper atmosphere, computed as $T_{ul} = T_a - \Gamma H_{ul}$, where H_{ul} is the distance from the middle to upper atmosphere. Note that the ϵ_a in the first term on the r.h.s. of Eq. A7 accounts for the fact that some surface longwave radiation is transmitted directly to space.

The sensible heat flux, F_s, is parameterized using a bulk coefficient, $F_s = K_s(T_s - T_{as})$. Likewise, the heat flux from the subsurface into the surface is parameterized as having a linear dependence on the temperature gradient, $F_{ss} = K_{ss}(T_s - T_{ss})$.

The eddy heat flux divergence depends on the meridional temperature gradient in the middle atmosphere [*Stone*, 1972],

$$D_a = \frac{\partial}{\partial \phi}\left(K_a \| \frac{\partial T_a}{\partial \phi} \| \frac{\partial T_a}{\partial \phi} \right), \tag{A8}$$

where $\|.\|$ indicates the absolute value, ϕ is latitude, and K_a is tuned to give a reasonable meridional heat flux.

One meter of precipitation falls annually in the model at each grid point and is equally distributed throughout the year. Precipitation collects as ice when the temperature of the atmospheric surface layer is below freezing, and is assumed to run-off otherwise. The simplifying assumption is made that evaporation and precipitation occur at the same latitude so that meridional latent heat fluxes are ignored. Ablation occurs when ice is present, the surface is at the melting point, and additional heat is fluxed into it. The amount of ablation is equal to the heat flux per square meter divided by the latent heat of ice per meter cubed. In this manner, ice tends to build up at high-latitudes during the winter and then ablate during the spring and summer. Precipitation which accumulates as ice is assumed to give up its excess heat to the atmosphere, so that ice accumulates on the ground with the same temperature as the atmospheric surface layer. A regression between ablation and positive degree days (see Eq. 1) calculated from the atmospheric boundary layer temperature yields a slope of 3mm/(°C day) — in good agreement with generally accepted values [e.g. *Braithwaite and Zhang*, 2000; *Lefebre et al.*, 2002].

A2. Icesheet

The icesheet component of the model is zonally averaged and a function of meridional distance, y, and height, z. It utilizes a common shallow-ice approximation [*van der Veen*, 1999, e.g.], assuming that deformation occurs only as a result of horizontal shear stress and that stress and strain are related by Glen's law. The ice is assumed isothermal and incompressible, and the evolution of its thickness is governed by the continuity equation,

$$\frac{\partial h}{\partial t} = B - \frac{\partial}{\partial y}(\bar{u}h). \tag{A9}$$

Here h is the thickness of the icesheet, B represents the surface mass-balance, and $\bar{u}$ is the vertically averaged velocity. The horizontal shear stress is approximated as a function of ice thickness and surface slope,

$$\tau_{yz} = -\rho_i g(h + H - z)\frac{\partial(h + H)}{\partial y}, \tag{A10}$$

where ρ_i is ice density and H is the elevation associated with the base of the icesheet. It follows that the horizontal velocity is,

$$u(z) = \frac{(\rho g)^n}{n-1} A \left(\frac{\partial(h+H)}{\partial y}\right)\left((h + H - z)^{(n+1)} - (h + H)^{(n+1)}\right) + u_b, \tag{A11}$$

where n is the exponent in Glen's flow law and A governs the deformability of the ice. A is known to depend on temperature, fabrics within the ice, and impurities [e.g. *Paterson*, 1994] but here, for simplicity, is taken as a constant, consistent with ice at a temperature of 270K. The final term, u_b, represents the velocity at the base of the ice-sheet owing to basal sliding or motion of subglacial sediment. Integrating u with respect to z and inserting into the continuity equation gives an expression for the temporal evolution of the icesheet,

$$\frac{\partial h}{\partial t} = B + \frac{\partial}{\partial y}\left(\frac{2A(\rho_i g)^n}{n+2}\left|\left(\frac{\partial(h+H)}{\partial y}\right)^{n-1}\right|\frac{\partial(h+H)}{\partial y}(h+H)^{n+2}\right| + u_b h). \tag{A12}$$

Basal velocity is prescribed according to the sediment deformation model of *Jenson et al.* [1996] and as used by *Clark and Pollard* [1998] (their Eq(3)). The velocity at the ice-sediment interface is,

$$u_b = \frac{2D_\circ a_{sed}}{(m+1)b_{sed}}\left(\frac{|a_{sed}|}{2D_o\mu_o}\right)^m\left(1 - \left[1 - \frac{b_{sed}}{|a_{sed}|}\min\left(h_s, \frac{|a_{sed}|}{b_{sed}}\right)\right]^{(m+1)}\right), \tag{A13}$$

where the vertical bars indicate the absolute value and "min" is the minimum of the two quantities. h_s is the thickness of the sediment at the base of the glacier. The value a_{sed} equals $\rho_i g h \partial(h+H)/\partial y$ and is the shear stress imparted from the ice into the sediment, and b_{sed} equals $(\rho_s - \rho_w) g \tan(\phi_s)$ and is the rate of increase of shear strength with depth in the sediment. The shear-zone thickness is given by the ratio a_{sed}/b_{sed}, and in the model of *Clark and Pollard* [1998] is typically between one and ten meters. We follow *Jenson et al.* [1996] and *Clark and Pollard* [1998] in assigning values for the sediment rheology. The angle of internal deformation is specified as $\phi_s = 22°$, the reference deformation rate is $D_o = 7.9 \times 10^{-7} s^{-1}$, the exponent m equals 1.25, and the reference viscosity is set $\mu_o = 3 \times 10^9$ Pa s. The appropriate value of μ_o is uncertain, and other experiments were conducted increasing and decreasing this value by an order of magnitude, and which yielded results qualitatively similar to those reported here.

The scouring of continental regolith is ignored, and a constant sediment thickness is assumed. Furthermore, the sediment is assumed to always be liquid saturated and thus readily deformed. Tracking the temperature and heat transport of the icesheet itself would permit a more realistic representation of basal melting and hydrology, though in this meridional icesheet the difficult subject of water drainage would, at best, still be crudely represented.

The adjustment of the bed height to the overlying ice load is modeled as a simple local relaxation toward isostatic equilibrium [e.g. *Clark and Pollard*, 1998],

$$\frac{\partial H}{\partial t} = \frac{1}{T_b}\left(H_{eq} - H - \frac{\rho_i h}{\rho_b}\right), \tag{A14}$$

where H is the height of the bed above sea-level, H_{eq} is the equilibrium height of the bed given ice-free conditions (taken as zero meters), h is the height of the ice above the bed, ρ_i is the ice-density (910 kg/m^3), ρ_b is the bedrock density (3370 kg/m^3), and T_b is a time-constant set to 5 Ky [following *Peltier and Marshall*, 1995; *Clark and Pollard*, 1998]. Ice flowing to 85°N is assumed to calve into the ocean and melt.

The icesheet influences the EBM in a variety of ways: the presence of ice changes the surface albedo in the EBM, the height of the ice-sheet influences surface temperature according to the moist adiabatic lapse rate, and the latent heat in the ice can cause large surface-atmosphere temperature contrasts. Likewise, the EBM feeds back onto the icesheet through determining the surface mass balance. The EBM and icesheet components are asynchronously coupled. The EBM is stepped forward at fifteen minute intervals for five years using the Euler method, and the glacial mass balance is calculated from the difference in accumulation and ablation averaged over the final year of the EBM run. The ice-model is then integrated forward for 500 years using a semi-implicit Crank-Nicholson formulation at 5 year time-steps, after which the energy-balance model is again run to equilibrium with the new ice distribution. Integrations using different time-stepping, up to 1 day time-steps in the EBM run for 3 to 25 year intervals and 1 to 5 year time steps in the ice-sheet model run for intervals of 50 to 500, yield essentially identical results indicating that the time-stepping and coupling techniques are stable. Model runs are started at 2.1 Ma. Runs starting from different initial conditions all converge by 2 Ma.

A3. Model climate

Under the modern orbital configuration, no ice accumulates and the model equilibrates on a time-scale of years. Fig. 10 shows the seasonal cycles in various quantities contoured as a function of latitude. Surface temperatures are too warm in the tropics at 40°C, presumably owing to the model lacking evaporation, latent heat transport, and a Hadley circulation. Note that we are not attempting a realistic simulation, but rather to diagnose and isolate mechanisms responsible for the 40 Ky glacial cycles within a model containing only the most pertinent physics. Extra-tropical temperatures, which are by far the more important for glaciation in this model, are more in keeping with observations, decreasing to an annual average of -15°C at 85°N.

Accumulation occurs throughout the winter in high latitudes, with a longer accumulation season at the highest latitudes. In unglaciated conditions, ablation occurs primarily in the spring and, at high latitudes, extends into the summer, keeping surface cool later into the year. The mid-troposphere temperature undergoes a more symmetric seasonal cycles than at the surface, inducing large heat fluxes into the surface during the ablation season. The subsurface temperature adjusts more slowly, having a seasonal cycles which is lagged and attenuated relative to the surface, and tending to warm the surface in the winter and cool it in the summer.

Instrumental records of temperature show that daily average insolation intensity has an almost perfectly linear relationship with zonally averaged surface air temperatures when they are lagged relative to the insolation time-series by 30 days [*Huybers*, 2006]. The model shows a similar relationship, where the cross-correlation between insolation and temperature lagged by 30 days is 0.99 or greater at all extra-tropical latitudes. Note, however, that when parts of the model become glaciated, surface ground temperatures cannot exceed the melting point, tending to suppress the atmospheric temperature and leading to a weaker correlation between insolation and lagged temperature of 0.9.

It is also useful to compute some seasonally averaged quantities which can be directly compared against modern observations [e.g. *Peixoto and Oort*, 1992]. In the model the meridional transport of heat peaks at 4 Peta-watts at 50°N (fig 11b), whereas modern estimates of heat transport peak at 5 Peta-watts near 30°N [*Trenberth and Caron*, 2001]. The northerly peak in heat transport owes to absorption of heat by the seasonal snow cover, and the weaker heat transport at lower latitudes presumably owes to lack of latent and Hadley cell heat transports in the model.

Two different albedos are specified in the model for ice (0.8) and bare land (0.3). The annual average albedo in the model is 0.3 at low-latitudes but increases beginning in the mid-latitudes to values of 0.8 at the permanent sea-ice parameterized for latitudes above 85°N. The average albedo during winter is significantly higher in the mid and high-latitudes owing to the presence of ice cover, and are commensurate with those estimated for Greenland and Antarctica. Estimates of zonal average albedo for the modern climate are similar to those produced by the model [*Peixoto and Oort*, 1992].

The total absorbed solar radiation (Fig. 11d) is a function of the incident radiation; the albedo of the surface; and the atmospheric transmissivity, reflectivity, and absorptivity. The annual average absorbed solar radiation is 250 W/m^2 in the tropics and steadily decreases to about 100 W/m^2 in the Arctic. The emitted terrestrial radiation in the model

(Fig. 11e) is somewhat less than 250 W/m^2 at the equator and somewhat more than 100 W/m^2 at the pole, but values are all within approximately 30 W/m^2 of those estimated for the modern climate [*Peixoto and Oort*, 1992]. The difference between the absorbed and emitted radiation (Fig. 11f) owes to local heat storage as well as the atmospheric transport of heat. In the arctic, the model atmospheric heat flux convergence is 30 W/m^2 on an annual average basis but can reach as high as 90 W/m^2 during polar night. Overall, we conclude that the EBM gives a sufficiently reasonable representation of the seasonal cycle to permit exploration of the mechanisms connecting insolation to ice-volume fluctuations.

References

Alley, R., Deforming-bed origin for southern Laurentide till sheets?, *Journal of Glaciology*, *37*, 67–75, 1991.

Ashkenazy, Y., and E. Tziperman, Are the 41 kyr glacial oscillations a linear response to Milankovitch forcing?, *Quaternary Science Reviews*, *23*, 1879–1890, doi:10.1016/j.quascirev.2004.04.008, 2004.

Barendregt, R., and E. Irving, Changes in the extent of North American ice sheets during the late Cenozoic, *Canadian Journal of Earth Science*, *35*, 504–509, 1998.

Beget, J., Influence of till rheology on pleistocene glacier flow in southern Great Lakes area, U.S.A., *Journal of Glaciology*, *32*, 235–241, 1986.

Berger, A., Long-term variations of daily insolation and Quaternary climatic changes, *Journal of Atmospheric Sciences*, *35*, 2362–2367, 1978.

Berger, A., and M. F. Loutre, Astronomical solutions for paleoclimate studies over the last 3 million years, *Earth Planet. Sci. Lett.*, *111*, 369–382, 1992.

Berger, A., and M. F. Loutre, Long-term variations in insolation and their effects on climate, the LLN experiments, *Surv. Geophys.*, *18*, 147–161, 1997.

Boellstorff, J., North American Pleistocene stages reconsidered in light of probable Pliocene-Pleistocene continental glaciation, *Science*, *202*, 305–307, 1978.

Braithwaite, R., and Y. Zhang, Sensitivity of mass balance of five swiss glaciers to temperature changes assessed by tuning a degree-day model, *Journal of Glaciology*, *152*, 7–14, 2000.

Clark, P., and D. Pollard, Origin of the middle Pleistocene transition by ice sheet erosion of regolith, *Paleoceanography*, *13* (1), 1–9, 1998.

DeConto, R., and D. Pollard, A coupled climate-ice sheet modeling approach to the early Cenozoic history of the Antarctic ice sheet, *Palaeogeography, Palaeoclimatology, Palaeoecology*, *198*, 39–52, 2003a.

DeConto, R., and D. Pollard, Rapid Cenozoic glaciation of Antarctica induced by declining atmospheric CO2, *Nature*, *421*, 245–249, 2003b.

Dwyer, G., P. Baker, and T. Cronin, North Atlantic deepwater temperature change during late Pliocene and late Quaternary climatic cycles, *Science*, *270*, 1347–1350, 1995.

Fisher, D., N. Reeh, and K. Langley, Objective reconstructions of the late Wisconsin Laurentide ice sheet and the significance of deformable beds, *Geographie Physique et Quaternaire*, *39*, 229–238, 1985.

Ghil, M., Cryothermodynamics: the chaotic dynamics of paleoclimate, *Physica D*, *77*, 130–159, 1994.

Gildor, H., and E. Tziperman, Sea ice as the glacial cycles' climate switch: Role of seasonal and orbital forcing, *Paleoceanography*, *15*, 605–615, 2000.

Goody, R., *Principles of Atmospheric Physics and Chemistry*, Oxford University Press, 1995.

Hagelberg, T., N. Pisias, and S. Elgar, Linear and nonlinear couplings between orbital forcing and the marine δ^{18}O record, *Paleoceanography*, *6*, 729–746, 1991.

Hays, J., J. Imbrie, and N. Shackleton, Variations in the earth's orbit: Pacemaker of the ice ages, *Science*, *194*, 1121–1132, 1976.

Huybers, P., Early pleistocene glacial cycles and the intergrated summer insolation forcing, *Science*, *313*, 508–511, 2006.

Huybers, P., Glacial variability over the last 2Ma: an extended depth-derived agemodel, continuous obliquity pacing, and the Pleistocene progression, *Quat. Sci. Rev.*, *26*, 37–55, 2007.

Huybers, P., and C. Wunsch, A depth-derived Pleistocene age-model: Uncertainty estimates, sedimentation variability, and nonlinear climate change, *Paleoceanography*, *19*, 10.1029/2002PA000,857, 2004.

Huybers, P., and C. Wunsch, Obliquity pacing of the late-Pleistocene glacial cycles, *Nature*, *434*, 491–494, 2005.

Imbrie, J., and J. Imbrie, Modeling the climatic response to orbital variations, *Science*, *207*, 943–953, 1980.

Imbrie, J., et al., On the structure and origin of major glaciation cycles. 1. Linear responses to Milankovitch forcing, *Paleoceanography*, *7*, 701–738, 1992.

Imbrie, J., et al., On the structure and origin of major glaciation cycles .2. The 100,000-year cycle, *Paleoceanography*, *8*, 699–735, 1993.

Jackson, C., and A. Broccoli, Orbital forcing of arctic climate: mechanisms of climate response and implications for continental glaciation, *Climate Dynamics*, *21*, 539–557, doi:DOI 10.1007/s00382-003-0351-3, 2003.

Jansen, E., T. Fronval, F. Rack, and J. Channell, Pliocene-Pleistocene ice rafting history and cyclicity in the nordic seas during the last 3.5 myr, *Paleoceanography*, *15*, 709–721, 2000.

Jenson, J., D. MacAyeal, P. Clark, and C. Ho, Numerical modeling of subglacial sediment deformation: Implications for the behavior of the Lake Michigan lobe, Laurentide ice sheet, *Journal of Geophysical Research*, *101*, 8717–8728, 1996.

Johnson, R., Major northern hemisphere deglaciation caused by a moisture deficit 140 ka, *Geology*, *19*, 686–689, 1991.

Joyce, J., L. Tjalsma, and J. Prutzman, North American glacial meltwater history for the past 2.3 m.y.: Oxygen isotope evidence from the Gulf of Mexico, *Geology*, *21*, 483–486, 1993.

Kukla, J., The Pleistocene epoch and the evolution of man — a reply, *Current Antrhopology*, *9*, 24–47, 1968.

Lawrence, K., Z. Liu, and H. T., Evolution of the eastern tropical Pacific through Plio-Pleistocene glaciation, *Science*, *312*, 79–83, 2006.

Lefebre, F., H. Gallee, J. Van Ypersele, and P. Huybrechts, Modelling of large-scale melt parameters with a regional climate model in south-Greenland during the 1991 melt season, *Annals of Glaciology*, *35*, 391–397, 2002.

Lisiecki, L., and M. Raymo, Plio-Pleistocene climate evolution: Trends and transitions in glacial cycle dynamics, *Quaternary Science Reviews*, *26*, 56–69, 2007.

Liu, Z., and T. Herbert, High latitude signature in Eastern Equatorial Pacific climate during the early Pleistocene epoch, *Nature*, *427*, 720–723, 2004.

McIntyre, S., A. Ravelo, and M. Delaney, North Atlantic intermediate waters in the late Pliocene to early Pleistocene, *Paleoceanography*, *14*, 324–335, 1999.

Milankovitch, M., *Kanon der Erdbestrahlung und seine Andwendung auf das Eiszeitenproblem*, Royal Serbian Academy, Belgrade, 1941.

Muller, R., and G. MacDonald, *Ice Ages and Astronomical Causes*, Springer, 2000.

Nisancioglu, K., Modeling the impact of atmospheric moisture transport on global ice volume, Ph.D. thesis, MIT, 2004.

North, G., R. Cahalan, and J. Coakley, Energy balance climate models, *Reviews of Geophysics and Space Physics*, *19*, 91–121, 1981.

Oerlemans, J., Model experiments on the 100,000-yr glacial cycle, *Nature*, *4287*, 430–432, 1980.

Oerlemans, J., Glacial cycles and ice-sheet modelling, *Climatic Change*, *4*, 353–374, 1984.

Paterson, W., *Physics of Glaciers*, 3rd ed., Pergamon Press, 1994.

Peixoto, J., and A. Oort, *Physics of Climate*, American Institute of Physics, 1992.

Peltier, W. R., and S. Marshall, Coupled energy-balance/icesheet model simulations of the glacial cycles: A possible connection between terminations and terrigenous dust, *Journal of Geophysical Research*, *100*, 14,269–14,289, 1995.

Pillans, B., J. Chappell, and R. Naish, A review of the Milankovitch climatic beat: template for PlioPleistocene sea-level changes and sequence stratigraphy, *Sedimentary Geology*, *122*, 5–21, 1998.

Pisias, N., and T. Moore, The evolution of Pleistocene climate: a time series approach, *Earth and Planetary Science Letters*, *52*, 450–458, 1981.

Pollard, D., An investigation of the astronomical theory of ice ages using a simple climate-ice sheet model, *Nature*, *272*, 233–235, 1978.

Pollard, D., A simple ice sheet model yields realistic 100 kyr glacial cycles, *Nature*, *296*, 334–338, 1982.

Ravelo, A., D. Andreasen, M. Lyle, A. Lyle, and M. Wara, Regional climate shifts caused by gradual global cooling in the Pliocene epoch, *Nature*, *429*, 263–267, 2004.

Raymo, M., The initiation of Northern Hemisphere glaciation, *Annual Reviews of Earth and Planetary Science*, *22*, 353–383, 1994.

Raymo, M., and K. Nisancioglu, The 41 kyr world: Milankovitch's other unsolved mystery, *Paleoceanography*, *18(1)*, 10.1029/2002PA000,791, 2003.

Raymo, M., W. Ruddiman, J. Backman, B. Clement, and D. Martinson, Late Pliocene variations in Northern Hemisphere ice sheets and North Atlantic deep water circulation, *Paleoceanography*, *4*, 413–446, 1989.

Raymo, M., L. Lisiecki, and K. Nisancioglu, Plio-Pleistocene ice volume, Antarctic climate, and the global δ^{18}o record, *Science*, *313*, 10.1126/science.1123,296, 2006.

Roe, G., In defense of Milankovitch, *Geophysical Research Letters*, *33*, L24703, 10.1029/2006GL027817, 2006.

Rubincam, D., Insolation in terms of Earth's orbital parameters, *Theoretical Applied Climatology*, *48*, 195–202, 1994.

Ruddiman, W. F., M. Raymo, D. Martinson, B. Clement, and J. Backman, Pleistocene evolution: Northern Hemisphere ice sheets and the North Atlantic Ocean, *Paleoceanography*, *4*, 353–412, 1989.

Shackleton, N. J., and M. Hall, Oxygen and carbon isotope stratigraphy of Deep-Sea Drilling Project hole 552a: Plio-Pleistocene glacial history, *DSDP Initial Reports*, *81*, 599–609, 1984.

Shackleton, N. J., and N. D. Opdyke, Oxygen-isotope and paleomagnetic stratigraphy of Pacific core V28-239: Late Pliocene to latest Pleistocene, *Mem Geol. Soc, Am.*, *145*, 449–464, 1976.

Shell, K., and R. Somerville, A generalized energy balance climate model with parameterized dynamics and diabatic heating, *Journal of Climate*, *18*, 1753–1772, 2005.

Stone, P., A simplified radiative-dynamical model for the static stability of rotating atmospheres, *Journal of Atmospheric Science*, *29*, 405–418, 1972.

Tiedemann, R., M. Sarnthein, and N. J. Shackleton, Astronomic timescale for the Pliocene Atlantic δ^{18}O and dust flux records of ODP site 659, *Paleoceanography*, *9*, 619–638, 1994.

Trenberth, K., and J. Caron, Estimates of meridional atmosphere and ocean heat transports, *Journal of Climate*, *14*, 3433–3443, 2001.

Tziperman, E., M. Raymo, P. Huybers, and C. Wunsch, Consequences of pacing the Pleistocene 100 kyr ice ages by nonlinear phase locking to Milankovitch forcing, *Paleoceanography*, *21*, PA4206, 10.1029/2005PA001241, 2006.

van der Veen, C., *Fundamentals of Glacier Dynamics*, A.A. Balkema, 1999.

Venz, K., D. Hodell, C. Stanton, and D. Warnke, A 1.0 Myr record of glacial North Atlantic intermediate water variability from ODP site 982 in the Northeast Atlantic, *Paleoceanography*, *14*, 42–52, 1999.

Weertman, J., Milankovitch solar radiation variations and ice age ice sheet size, *Nature*, *261*, 17–20, 1976.

Young, M., and R. Bradley, Insolation gradients and the paleoclimatic record, in *Milankovitch and Climate, Part 2*, edited by A. Berger and et. al., pp. 707–713, D. Riedel, Hingham, Mass., 1984.

Zachos, J., M. Pagani, L. Sloan, E. Thomas, and K. Billups, Trends, rhythms, and aberrrations in global cliamte 65Ma to present, *Science*, *292*, 686–693, 2001.

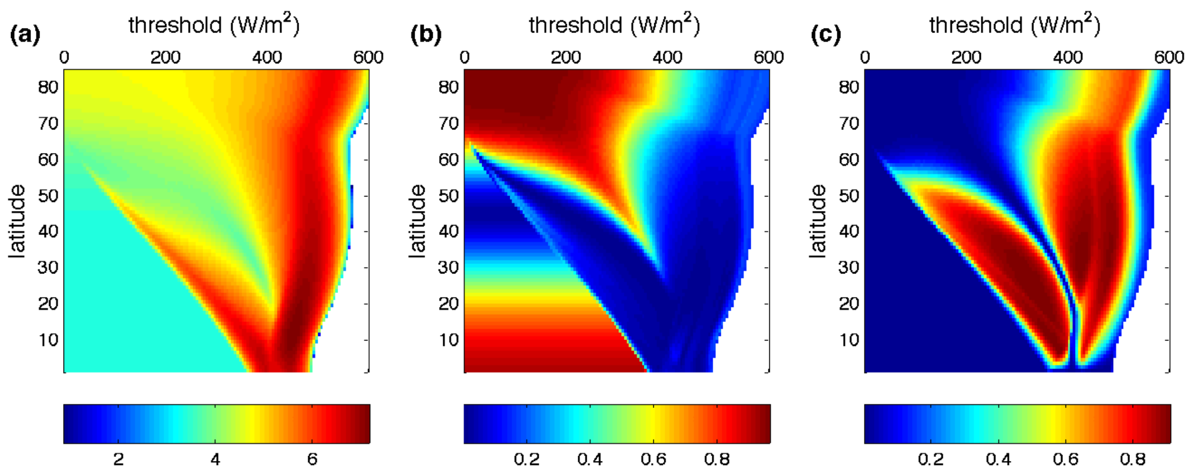

Figure 1. Summer-energy variability as a function of latitude and threshold. **(a)** The variance of the summer-energy contoured in units of $\log_{10}$(Giga-Joules/m^2)^2. **(b)** The fraction of summer-energy variance occuring at the obliquity band (1/41±1/150 Ky^{-1}), and **(c)** the fraction of variance at the precession band (1/21±1/150 Ky^{-1}). Together, the obliquity and precession bands account for over 90% of the summer-energy variance, with the remainder associated with eccentricity and the first over-tone of precession, i.e. ∼11Ky. Only the Northern Hemisphere is shown — values are symmetric for the Southern hemisphere. Representative time-series of summer-energy, as well as software to calculate insolation and summer-energy, can be downloaded at http://www.ncdc.noaa.gov/paleo/pubs/huybers2006b.

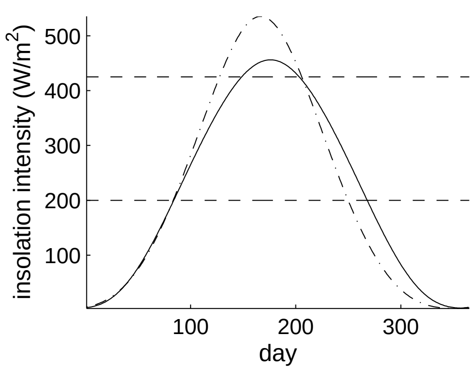

Figure 2. The seasonal cycle in daily average intensity at 65°N for perihelion occuring at Northern Hemisphere summer solstice (dashed-dot line) and at winter solstice (solid line). Two thresholds are indicated at 200 W/m^2 and 425 W/m^2. For the lower threshold, the summer-energy is insensitive to changes in precession (the intensity is counterbalanced by changes in duration), while the higher threshold gives a summer-energy sensitive primarily to precession.

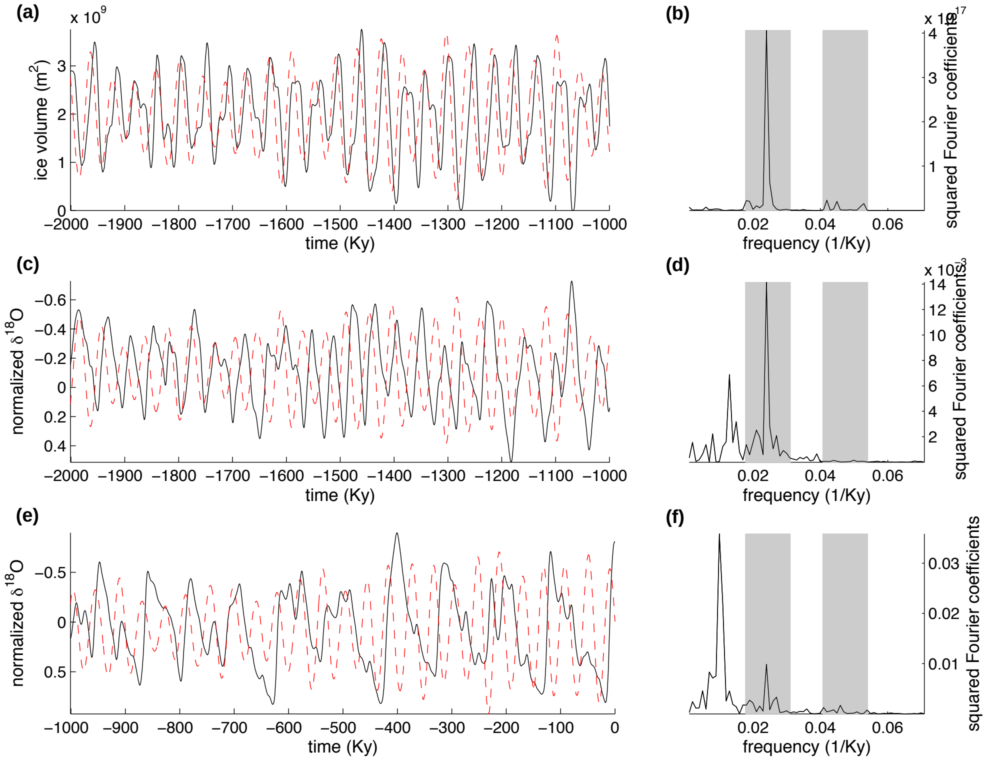

Figure 3. Glacial variability during the early Pleistocene. **(a)** Model ice-volume (actually area since the ice-model only represents latitude and height) calculated as the meridional integral of the icesheet height as a function of time. Note that time runs from left to right. The dashed line is the Earth's obliquity, but with its sign reversed and mean and variance adjusted to match that of the ice-volume. **(b)** Periodogram of the ice-volume with the obliquity ($1/41 \pm 1/100$ Ky^{-1}) and precession ($1/22 \pm 1/100$ Ky^{-1}) bands shaded. For reference, the variations in benthic δ^{18}O and their periodogram are shown for **(c,d)** the early Pleistocene and **(e,f)** the late Pleistocene. δ^{18}O values have their time-mean removed and are pinned to a depth-derived age-model, not relying on orbital assumptions [see *Huybers*, 2007].

Variable	Value	Units	Description
a	6.37^6	m	Radius of the earth
K	273.15	K	Melting point
ρ_i	900	Kg/m^3	Density of ice
ρ_w	1000	Kg/m^3	Density of water
ρ_a	1.5	Kg/m^3	Surface air density
K_{ss}	2	J/(m K s)	Thermal conductivity between surface and subsurface
g	9.8	m/s^2	Acceleration of gravity
σ	5.67e-8	W/(m^{2}K^4)	Stefan Boltzmann constant
L_v	2.5×10^6	J/kg	Latent heat of vaporization
L_m	3.34×10^5	J/kg	Latent heat of melting
L_s	2.84×10^6	J/kg	Latent heat of sublimation
C_p	2100	J/(kg K)	Specific heat capacity of water
C_{air}	1.5	J/(kg K)	Specific heat capacity of air
C_{ss}	$10\rho_i C_p$	J/(m^{2}K)	Subsurface heat capacity
C_s	$5\rho_i C_p$	J/(m^{2}K)	Surface heat capacity
C_a	$5000\rho_a C_{air}$	J/(m^{2}K)	Atmospheric Heat capacity
K_s	5	J/K	Sensible heat flux
K_a	1000/(degree latitude)	J/K	Meridional heat flux coefficient
H_{as}	5	km	Height of middle atmosphere above sea-level
H_{ul}	2	km	Upper atmosphere thickness
α_g	0.3	—	land albedo
α_i	0.8	—	ice albedo
A	0.2	—	Absorption of atmosphere
R	0.3	—	Reflection of atmosphere
T	0.5	—	Transmission of atmosphere
ϵ_a	0.85	—	Longwave atmospheric emissivity
P	1	m/yr	Precipitation
Γ_m	6.5	K/km	Moist adiabatic lapse rate

Table 1. Parameters used for the energy balance model.

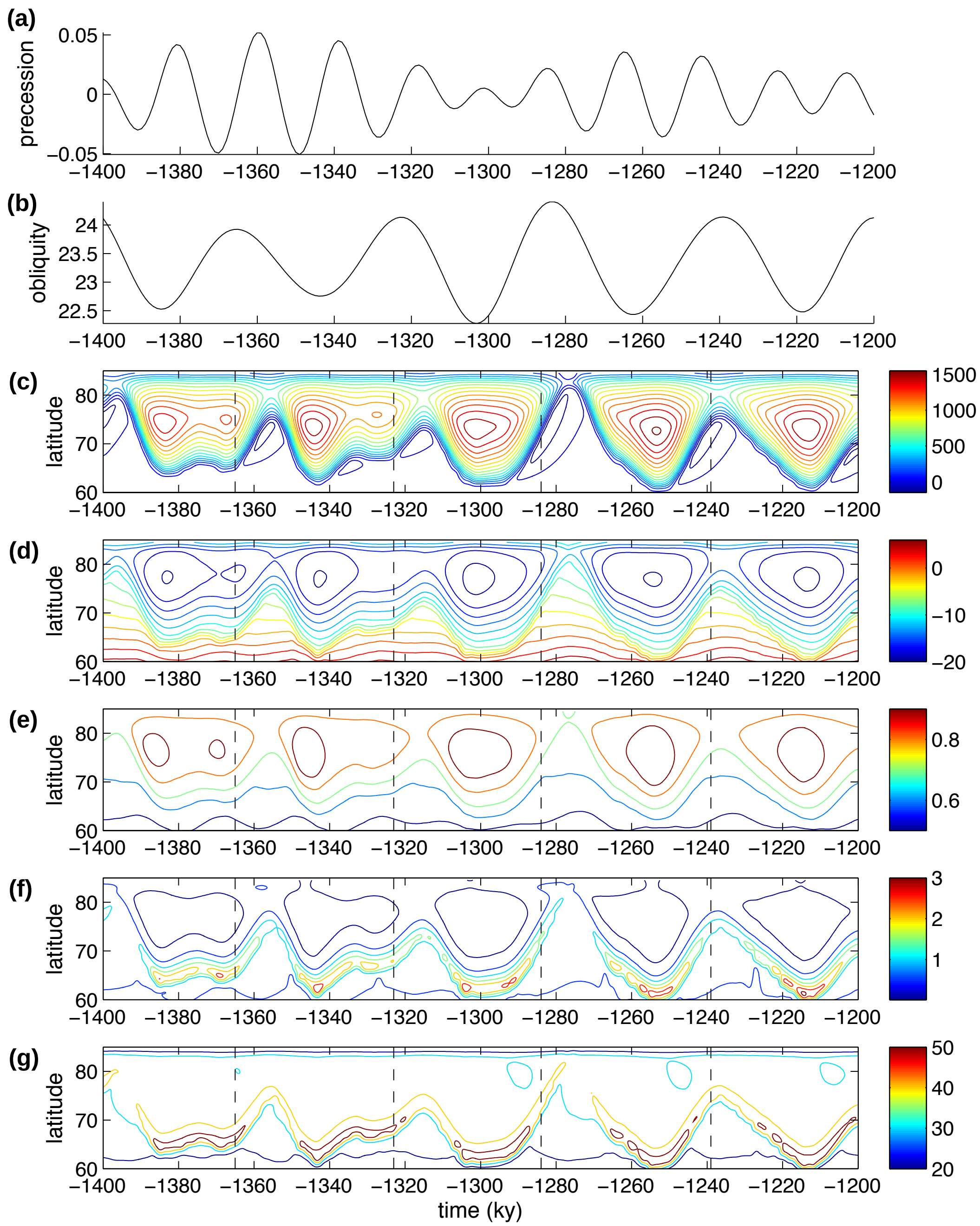

Figure 4. Time evolution of annual average model quantities. The climatic precession parameter **(a)** and Earth's obliquity **(b)** are shown for reference. **(c)** The height of the surface is contoured in 200 meter intervals. Negative values occur where ice has retreated from an isostatically depressed bed. Also shown are the annual average temperature (**d**, °C), accumulation (**e**, meters per year), ablation (**f**, meters per year), and total heat flux into the surface including short-wave, long-wave and sensible heating (**g**, W/m^2). Vertical lines indicate maxima in obliquity.

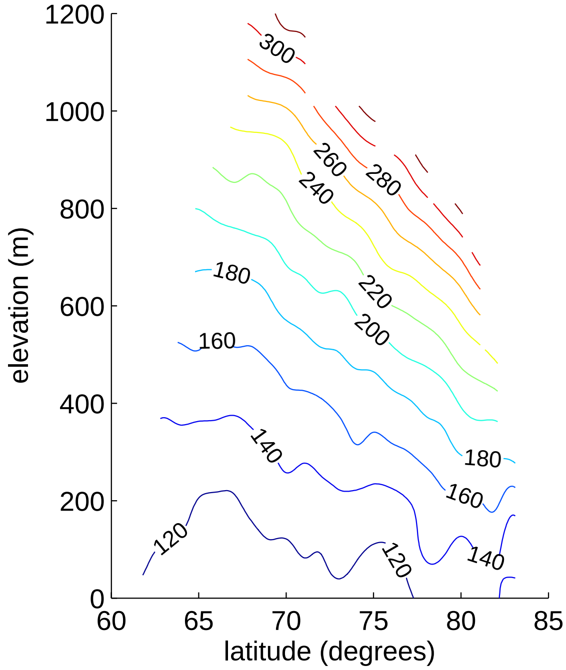

Figure 5. Insolation threshold for ablation to occur in the model. The threshold is diagnosed as the minimum diurnal average insolation intensity for which ablation occurs and is contoured as a function of latitude and elevation of the icesheet. Absence of contour lines indicates that no ablation occurs in this region. Note that the model insolation thresholds are within the domain for which summer-energy is obliquity dominated, i.e. $\tau < 350\mathrm{W/m}^2$ and a latitude above 60°N (see Fig. 1b).

Variable	Value	Units	Description
n	3	—	Exponent in Glen's law
A	7.7×10^{-29}	1/(Pa^3 s)	Deformability of the ice
T_b	5000	years	bed depression timescale
ρ_s	2390	kg/m^3	saturated bulk sediment density
ρ_b	3370	kg/m^3	bedrock density
ϕ_s	22°	degrees	angle of internal friction
D_o	2.5×10^{-14}	1/s	reference sediment deformation rate
m	1.25	—	Exponent in sediment stress-strain relationship
u_o	3×10^9	Pa/s	sediment reference viscosity
h_{sed}	10	m	thickness of sediment layer
H_{eq}	0	m	equilibrium height above sea-level
T_b	5000	yr	Bed relaxation time constant

Table 2. Parameters used for the ice-sheet and sediment model.

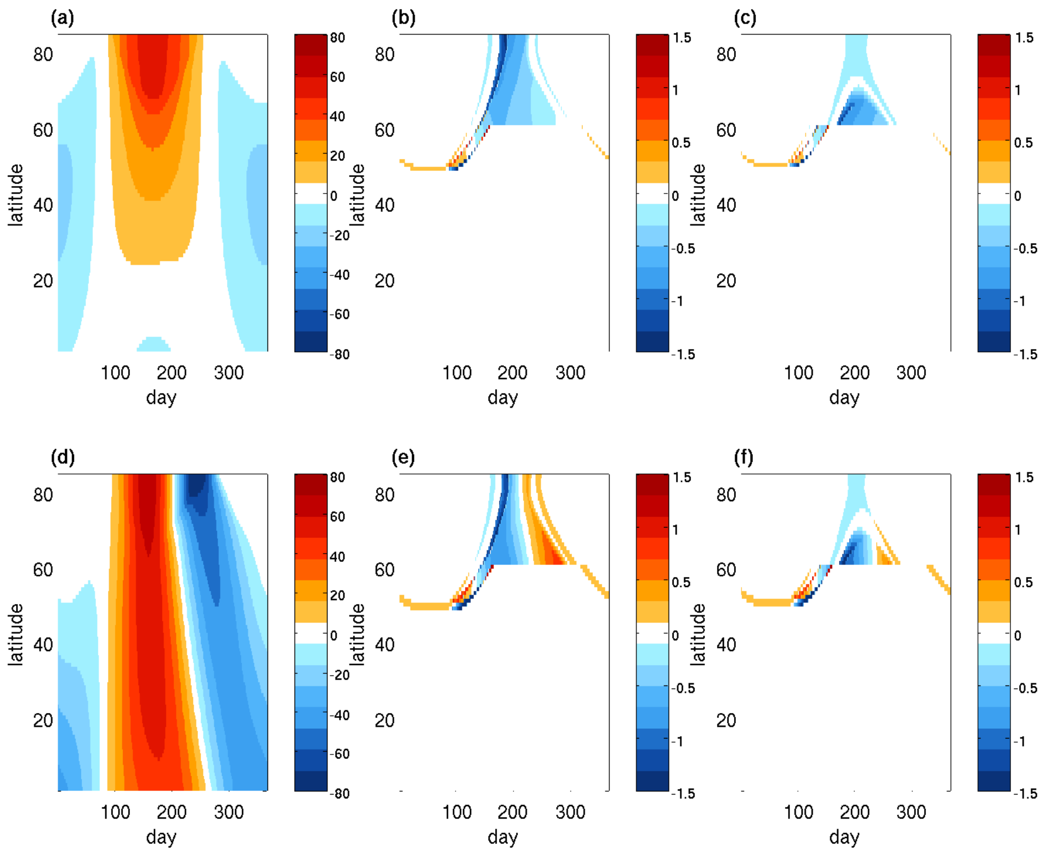

Figure 6. Orbitally induced variations in insolation and mass balance. **(a)** Difference in daily average insolation between maximum (24.5°) and minimum (22.1°) obliquity in W/m^2. The change in mass balance between maximum and minimum obliquity in meters per year for **(b)** an icesheet of uniform 10 meter thickness for latitudes above 60°N and **(c)** 1500 meter thickness. Lower panels are similar but for changing the location of perihelion from summer to winter solstice. All calculations are with an eccentricity of 0.0275 and, unless otherwise stated, an obliquity of 23.34° and perihelion occuring at vernal equinox. Note that for the thin icesheet the mass-balance anomalies associated with precession during summer and fall are opposite and of nearly equal magnitude, whereas for the thick and cooler icesheet the high-latitude anomaly is more uniform.

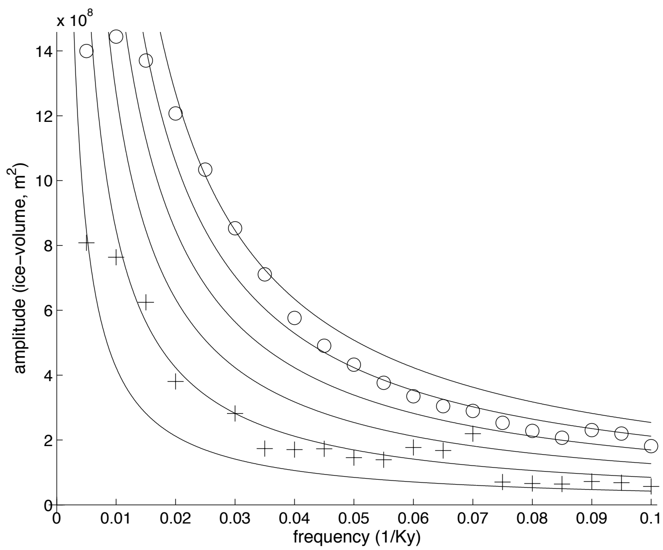

Figure 7. Glacial amplitude as a function of forcing frequency. Circles indicate the ice-volume amplitude resulting from sinusoidal changes in obliquity as a function of frequency. Crosses are similar but for the precession of the equinoxes. The actual obliquity and precession frequencies are 0.025 Ky^{-1} and 0.05 Ky^{-1} respectively. Solid lines indicate the expected change if amplitude is inversely proportional to frequency.

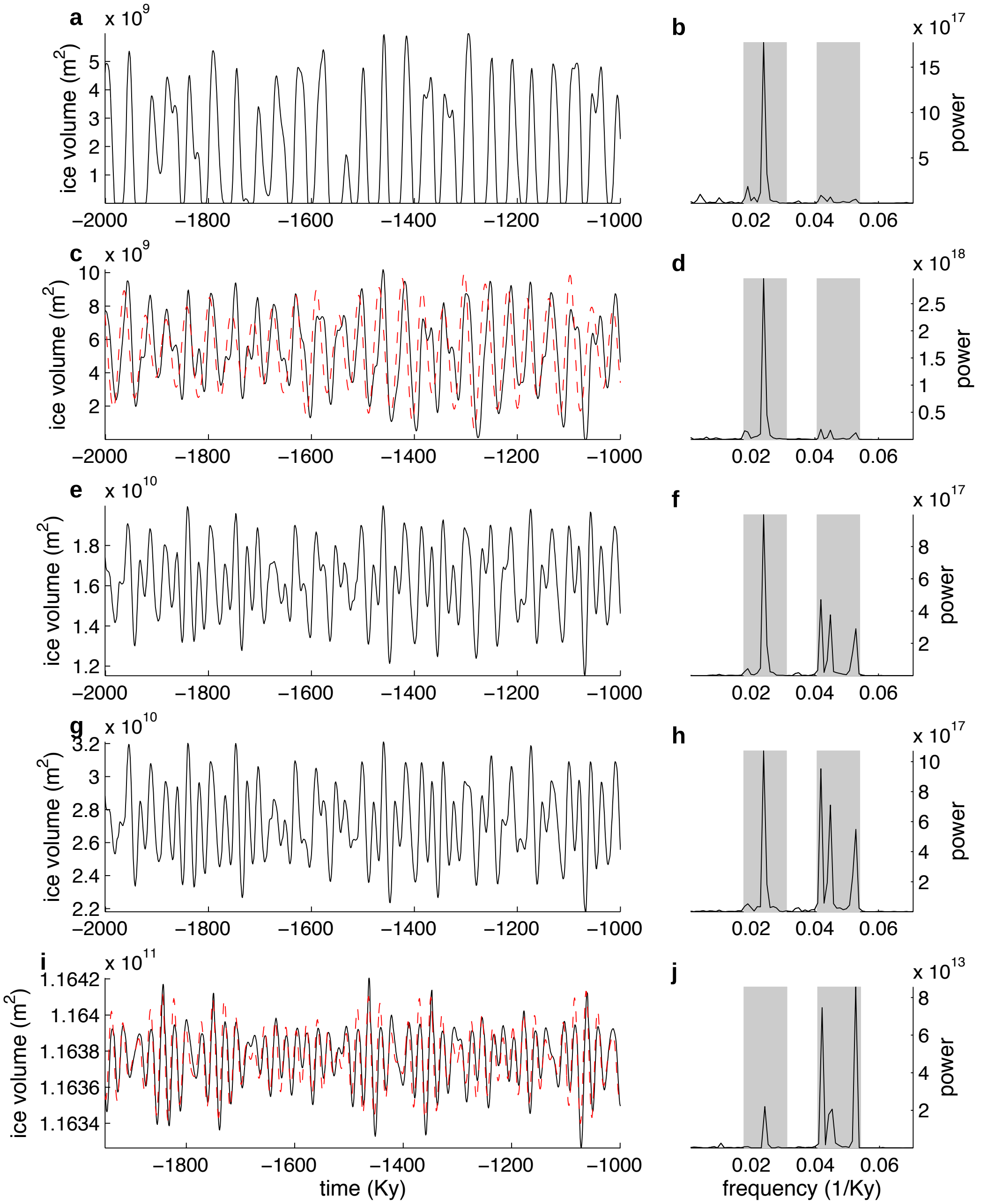

Figure 8. Glacial variability during the early Pleistocene under varying climate conditions. Panels **c** and **d** are the same as in Fig. 3a and b, showing the time variability of ice-volume and its periodogram respectively. The dashed line is obliquity with its sign reversed and mean and variance scaled. The shaded regions in the periodogram indicate the obliquity (left) and precession (right) bands. The other panels follow but with the emission height changed from 7Km to 7.1Km (**a,b**), 6.5Km **(e,f)**, and 6Km **(g,h)**. **(i,j)** depict the case when the emission level is at 7Km but in the absence of deformable basal sediment. In this case, ice-volume is primarily sensitive to precession, as indicated by the dashed line (again with reversed sign and scaled mean and variance). A cooler climate or thicker icesheet leads to greater precessional influence on ice volume. Note the y-axes have different limits, and that for the lower panels ice-volume variability is a small fraction of the total.

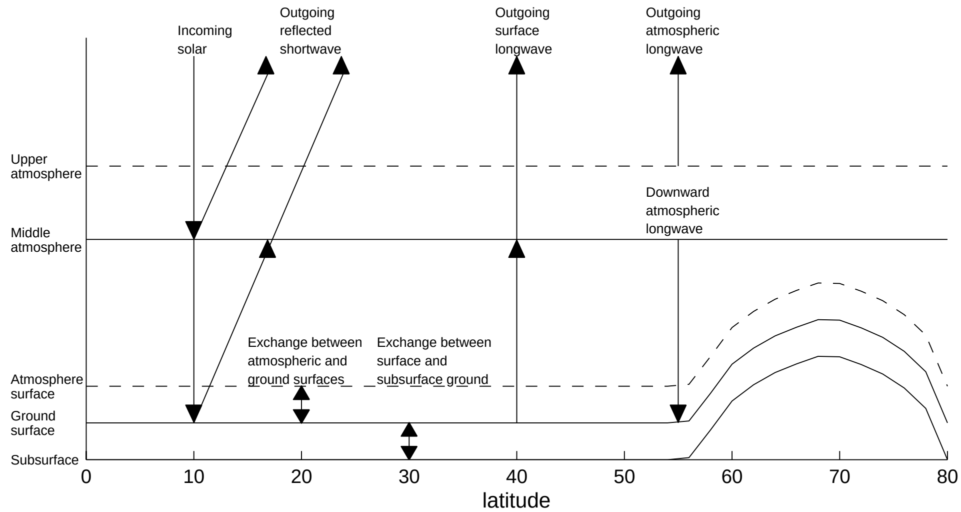

Figure 9. Schematic of the energy fluxes. Levels from top to bottom are the upper and middle atmosphere, atmospheric surface layer, ground/ice surface, and subsurface. Arrows indicate locations at which radiative, diffusive, or turbulent heat fluxes are absorbed or reflected. Note that the atmosphere radiates upward only at the upper atmospheric level. The model has one degree resolution in latitude. Surface and subsurface boxes are represented as either ground or ice and, in this case, an icesheet extends equatorward to 55°. For the sake of visual clarity, the y-axis is not drawn to scale.

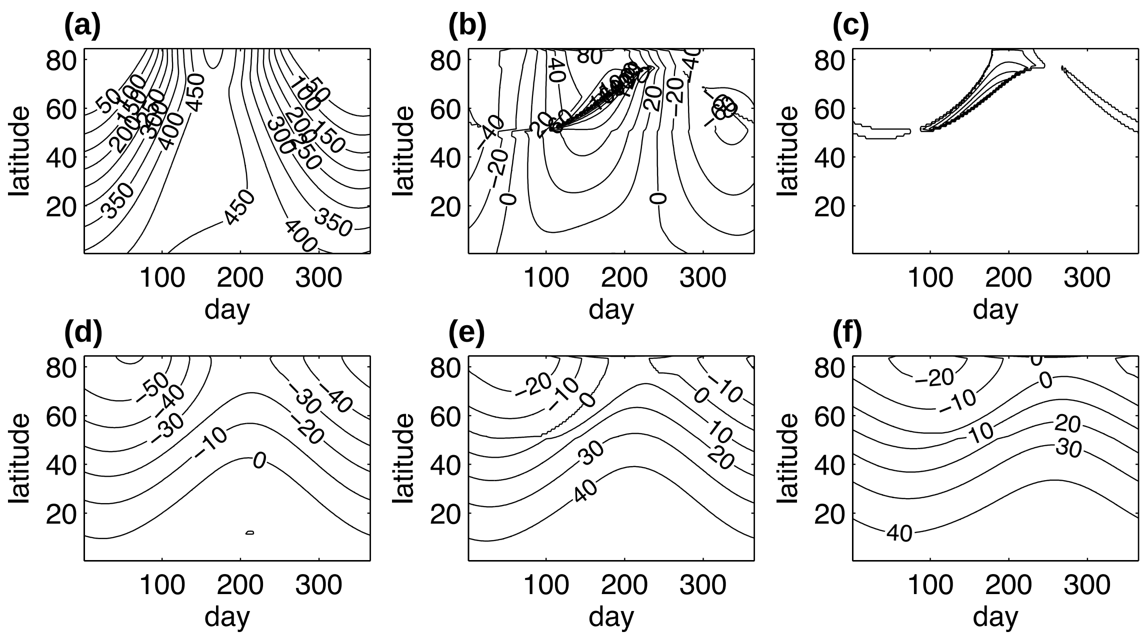

Figure 10. The annual cycle in the energy-balance model using the modern orbital configuration. Each quantity is contoured as a function of day of the year (starting with January 1st) and latitude. **(a)** Insolation at the top of the atmosphere in W/m^2. **(b)** The total heat flux across the land/atmosphere boundary — including sensible, shortwave and longwave heat fluxes in W/m^2. The densely spaced contour lines are in regions with snow and ice cover during the spring and summer and reach peak values of 220 W/m^2. **(c)** The rate of ablation with contours spaced by 2 cm/day. At bottom are the temperatures for **(d)** the middle atmosphere, **(e)** surface, and **(f)** subsurface in degrees Celsius.

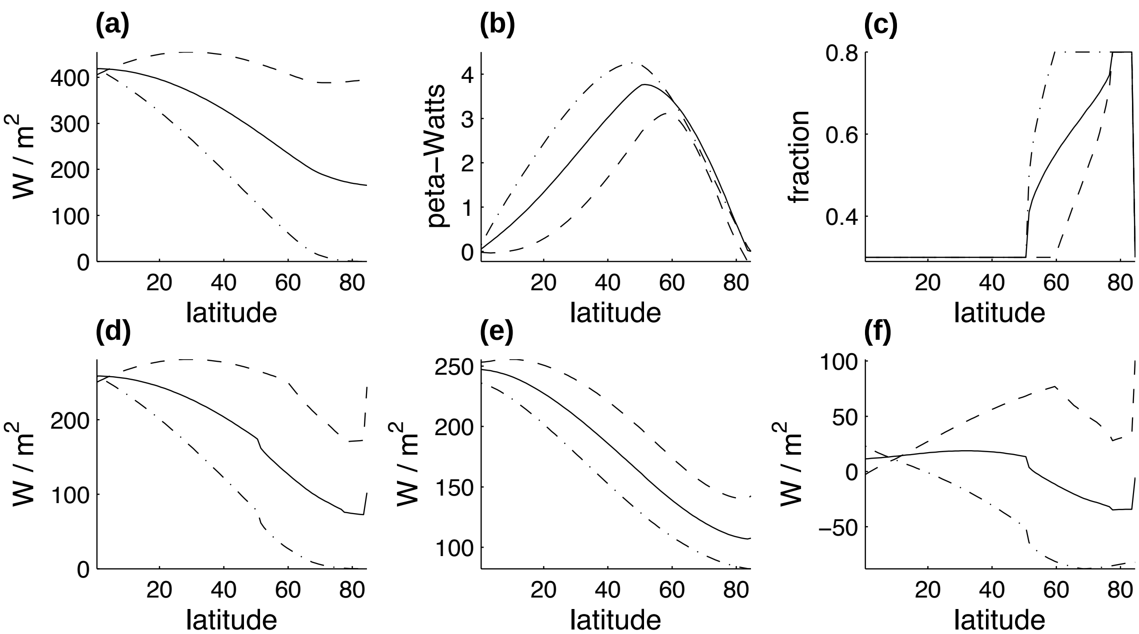

Figure 11. Model seasonal and annual averages of **(a)** incoming solar radiation, **(b)** atmospheric energy transport, **(c)** albedo, **(d)** absorbed solar radiation, **(e)** emitted terrestrial radiation, and **(f)** net heating. Solid lines are for the annual average, while dashed lines indicate summer (JJA) and dash-dot lines indicate winter (DFJ) averages. Values indicated in these plots can be directly compared with those estimated for the modern climate by *Peixoto and Oort* [1992, p127-129].